A Practical Spectroscopic and Theoretical Approach To Study the Electrochromism in Molecular-Based Materials: The Case of a Family of Dendrimerlike Poly(6-azulenylethenyl)benzenes

Juan Casado, Rocío Ponce Ortiz, and Juan T. López Navarrete*

Department of Physical Chemistry, University of Málaga, Campus de Teatinos s/n, Málaga 29071, Spain

Shunji Ito

Department of Materials Science and Technology, Faculty of Science and Technology, Hirosaki University, Hirosaki 036-8561, Japan

Noboru Morita

Department of Chemistry, Graduate School of Science, Tohoku University, Sendai 980-8578, Japan

Received: June 9, 2004

A series of branched poly(6-azulenylethenyl)benzene derivatives consisting of a central benzene ring surrounded by acetylene-bridged 1,3-bis(*n*-hexyloxycarbonyl) azulene arms has been investigated by physical and theoretical methods. Their optical and electrochemical features have been explained with the help of calculations regarding their π nature and extension of the lowest unoccupied molecular orbitals (LUMOs), the key factors that modulate their properties. The highest occupied molecular orbitals are located at the periphery of the molecules whereas their LUMOs also extend into the central core by which these molecules can be regarded as antennae systems. With an increase in the branching, the electronic structure of these molecules seems to be mostly affected at the level of the central phenyl core plus the acetylene bridges. The combination of Raman spectroscopy and calculations gives the possibility of analyzing particular geometrical and structural parameters otherwise hardly accessible by other techniques. Reduced species are characterized by double bond cumulated structures within the acetylenic spacers that give rise to a planarization of the molecules upon negative charging. Extensive intermolecular interactions, otherwise explaining their liquid crystalline behavior, both in solid state and in solution have been observed.

I. Introduction

Electrochromism is observed in reversible redox systems which exhibit significant color changes in different oxidation states.[1] Studies of the physical properties of organic molecules containing multiple redox-active chromophores are a fundamental step toward the ultimate preparation of new electrochromic materials that could be capable of tuning their visible absorption spectra (color) by changing their chemical architecture or the applied electrochemical potential.[2]

Ito et al. have prepared a series of polyelectrochromic materials using polyethynylbenzenes as a platform bearing multiple 1,3-bis(*n*-hexyloxycarbonyl) azulenes as redox-active moieties. The inclusion of the *n*-hexyloxycarbonyl chains infers good solubility, fusibility, and the ability to self-organize in columnar mesophases. In fact, these systems provide the first examples exhibiting multiple melting behavior and columnar mesomorphism in the chemistry of azulenes.[3−5] One can intuit that the redox abilities for these molecules are likely due to the notable tendency of azulene to stabilize anions. Furthermore, if the π-electron structure spreads over the entire system, then one might expect some modulation of the optical and electrochemical properties as a function of the substitution pattern and the applied potential or redox state. As an additional merit, these types of discotic materials have been exploited recently in optoelectronic (light-emitting diodes) devices due to their attractive electronic properties, in particular their remarkable charge transport abilities.[6]

The precise understanding of the structure−property relationships in molecular materials is of primary importance because the optimization of their electronic properties depends on how the electronic structure is related to the molecular or chemical functionalization. For instance, the electronic interactions between the conjugated building blocks of these macromolecules must be the responsible for tuning the redox potentials and the wavelength of the absorption bands of the neutral and the reduced forms. A useful and practical strategy for investigating these relationships is the analysis of some property as a function of the systematic variation in the number of repeat units in a given molecule.

Vibrational spectroscopy, and in particular Raman spectroscopy, is a very useful technique for studying the conjugational or π-electron delocalization properties of virtually any polyconjugated molecule because of, for example, the low number of Raman scatterings present in the spectra, which are selectively related to the π−electron delocalization features of the chromophore, the easy access to the spectra independent of the physical state of the sample, etc.[7−11] Herein our effort focuses on the combined use of vibrational spectroscopy and theoretical

* To whom correspondence should be addressed. E-mail: teodomiro@uma.es.

10.1021/jp047512a CCC: $27.50
Published on Web 11/10/2004

calculations for addressing molecular explanations of (i) the variation of the electronic structure of the molecules in neutral state upon increasing branching, (ii) upon electrochemical treatment or the reduced/oxidized species, and (iii) the changes on the spectra as a function of the temperature between −170 and 150 °C. For completeness, the electrochemical and optical features of the molecules are also addressed.

Therefore, for this work we will mainly use spectroscopy and quantum chemistry in order to explore the electronic structure of a series of poly(6-azulenylethenyl)benzene derivatives, focusing on the interactions between the peripheral groups and the core and on the role played by increasing the number of azulene groups. The suitability of Fourier transform Raman spectroscopy to deal with polyconjugated molecules regarding their electronic properties is the main reason we adopt this spectroscopic tool to evaluate the π-conjugational properties. The methodology first depends on the assignment of the Raman bands followed by the analysis of their wavenumber changes with the substitution pattern. Our final intention is to relate spectroscopic changes with the electronic features of the molecules with the help of theoretical calculations guided with the aim of giving molecular-scale insights for improving the electrochromic behavior of new materials.

II. Experimental and Theoretical Details

The synthesis of the azulene set of compounds has been reported elsewhere.[3,5a] The representative chemical structures for the molecules with acetylene bridges are displayed in Figure 1. Hereafter the 1,3-bis(*n*-hexyloxycarbonyl) azulene group will be termed as Az for clarity; A refers to the triple bond and Ph to the central phenyl ring. This work also deals with the homologous series lacking triple bonds that, however, have ethyl esters instead of hexyls. The UV−vis−near-IR spectra were recorded as CH_2Cl_2 solutions using a Perkin-Elmer Lambda 19 spectrometer. Electrochemical and spectroelectrochemical data were obtained in *o*-dichlorobenzene containing tetrabutylammonium tetrafluoroborate (0.1 M). FT-Raman spectra were measured using an FT-Raman accesory kit (FRA/106-S) for a Bruker Equinox 55 FT-IR interferometer. A continuous-wave Nd:YAG laser working at 1064 nm was employed for Raman excitation. A germanium detector operating at liquid-nitrogen temperature was used. Raman scattering radiation was collected in a backscattering configuration with a standard spectral resolution of 4 cm^{-1}. To avoid possible damage to the samples upon laser radiation, its power was kept at a level lower than 100 mW, and 1000 scans were averaged for each spectrum.

A variable-temperature cell Specac P/N 21525, with interchangeable pairs of quartz windows, was used to record the FT-Raman spectra at different temperatures. The variable-temperature cell consists of a surrounding vacuum jacket (0.5 Torr), and combines a refrigerant Dewar and a heating block as the sample holder. It is also equipped with a copper−constantan thermocouple for temperature monitoring purposes, and any temperature from −170 to 150 °C can be achieved. Samples were inserted into the heating block part or the Dewar/cell holder assembly in the form of pure solids in a quartz cell, and Raman spectra were recorded after waiting for thermal equilibrium in the sample, which required 20 min for every increment of 10 °C.

Full geometry optimizations were performed in the framework of the density functional theory (DFT) by means of the B3LYP functional, using the A.7 revision of the Gaussian 98 program package running on a SGI Origin 2000 computer.[12,13] The

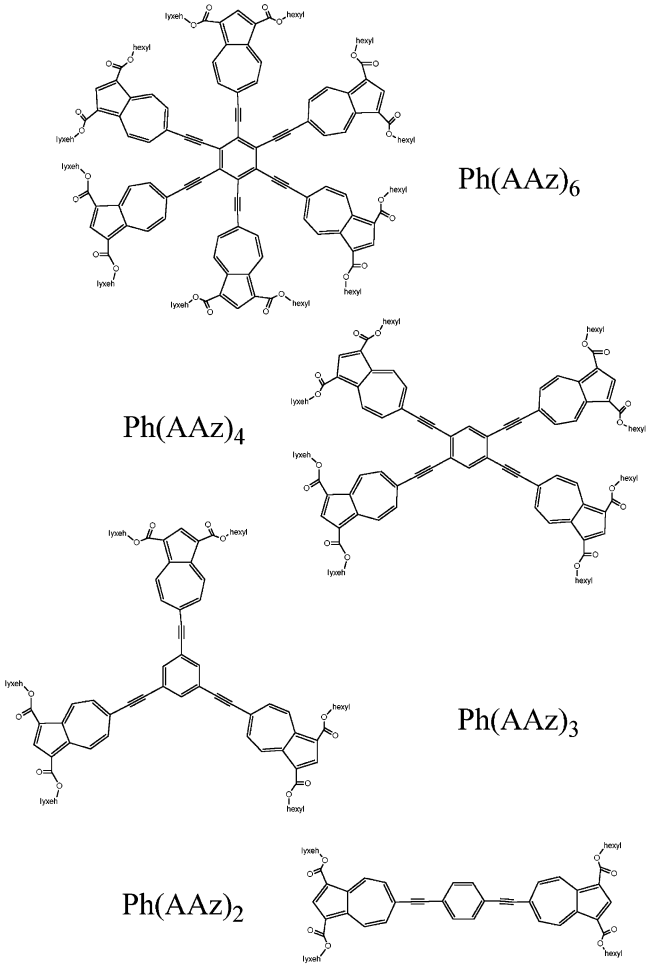

Figure 1. Representative chemical structures and nomenclature of the molecules.

6-31G** basis set was chosen as a compromise between the quality of the theoretical approach and the high computational cost associated with the high number of dimensions to the problem.[12,14] Due to the large molecular size of the compounds studied in this work, quantum chemical calculations were carried out on molecules with methyl groups instead of hexyl chains, being confident that these alkyl side chains have minimal effects on the conjugated path. Geometry optimizations were performed on isolated entities in the vacuum. All geometry parameters (i.e., bond lengths, bond angles, and dihedral angles) were allowed to vary independently along the molecular optimizations. For the charged species, no counterions were considered in the calculations. Vertical electronic excitation energies were computed by using the time-dependent density functional theory (TDDFT).[14] Numerical applications reported so far indicate that TDDFT employing the current exchange correlation functional performs significantly better than Hartree−Fock-based single excitation theories for the low-lying valence excited states. It has been demonstrated that the vibrational spectra calculated with the DFT methodology satisfactorily agree with experimental spectra in both relative intensities and peak positions.[12b] Because calculated vibrational spectra systematically overestimate frequency values due to electron correlation effects and basis set deficiencies, they must be properly corrected after inclusion of a uniform scaling factor of 0.96 as recommended by Scott and Radom.[12c] All of the quoted theoretical vibrational frequencies reported are thus scaled values.

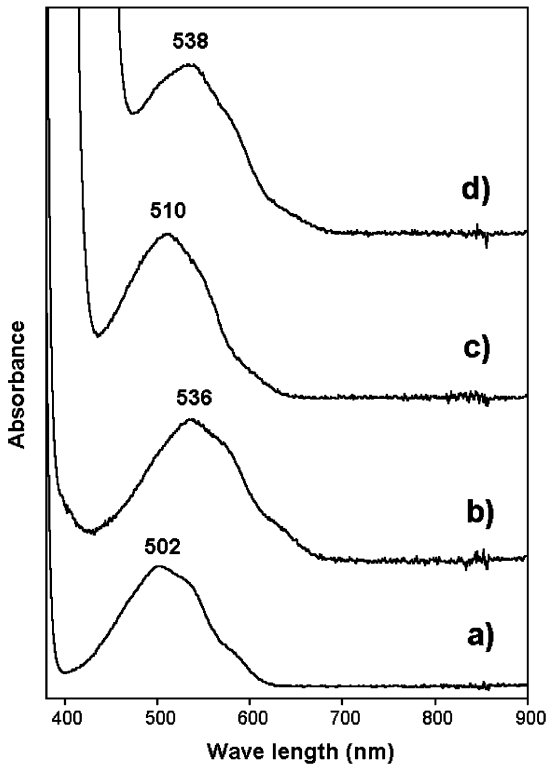

Figure 2. UV−vis−near-IR electronic spectra obtained in dichloromethane for (a) Az, (b) AAz, (c) $Ph(Az)_2$, and (d) $Ph(AAz)_2$.

III. Electronic Spectra

Figure 2 displays the UV−vis spectra of Az, AAz, $Ph(Az)_2$, and $Ph(AAz)_2$ in dichloromethane. TDDFT/B3LYP/6-31G** calculations of these molecules have been afforded to interpret their electronic absorption spectra. The longest wavelength in the spectrum of Az corresponds to the weak band at 502 nm, which is accompanied by two shoulders at higher energies, 526 and 573 nm, likely due to vibronic components. This band correlates with the theoretical feature at 475 nm, calculated with a low oscillator strength, $f = 0.0056$, and is described as an almost monoelectronic promotion from the highest occupied molecular orbital (HOMO) to the lowest unoccupied molecular orbital (LUMO). At 368 nm in the experimental spectrum, one intense band is measured that is assigned to a mixed HOMO − 1 → LUMO and HOMO → LUMO + 1 double promotion calculated at 349 nm with $f = 0.06$. Close to the last feature, a medium intensity band at 327 nm appears that is predicted at 287 nm with a oscillator strength of 0.0234. Finally, the strongest band of the spectrum at 296 nm is calculated at 267 nm, with $f = 0.7361$, due to multielectronic promotions.

The grafting of a triple bond to the Az group gives rise to an important 34 nm red shift of the HOMO−LUMO band, whereas for $Ph(Az)_2$ the HOMO−LUMO band is only red shifted by 8 nm relative to Az. Regarding $Ph(AAz)_2$, its longest wavelength electronic absorption at 538 nm is calculated at 548 nm (oscillator strength $f = 0.0062$) and described as a combination of different monoelectronic promotions that in decreasing order of contribution are: HOMO → LUMO, HOMO − 1 → LUMO, HOMO − 1 → LUMO + 1, and HOMO → LUMO + 1. Figure 3 displays the topology of the molecular orbitals involved in the above-mentioned transitions in $Ph(AAz)_2$, and Figure 4 schematically represents their absolute calculated energies. First, one observes that the HOMO (HOMO − 1 is degenerate) is located in the Az moiety; however, this is not the case for the LUMO, which spreads over the entire system. This charge-density delocalization accounts well for the progressive decrease in energy of the LUMOs when one successively grafts new fragments to the azulene, being especially important on passing from AAz to its phenyl dimmer. The contrary applies for the HOMO, restricted to the Az group, because it is only slightly stabilized after incorporation of the acetylene group although it remains almost isoenergetic in the $Ph(AAz)_2$ parent. As a forward consequence, the HOMO−LUMO energy difference is progressively narrowed, and therefore the electron absorption spectra is red shifted.

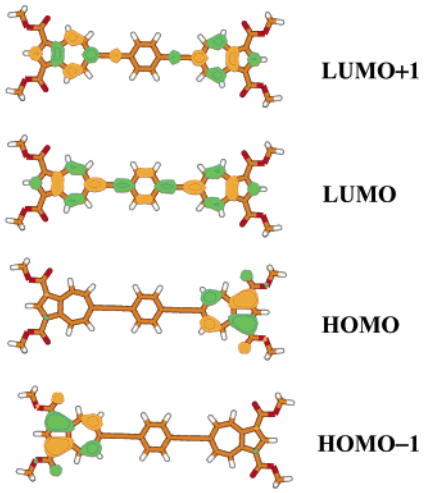

Figure 3. Frontier orbital topologies for $Ph(AAz)_2$ obtained by the DFT/B3LYP/6-31G** methodology.

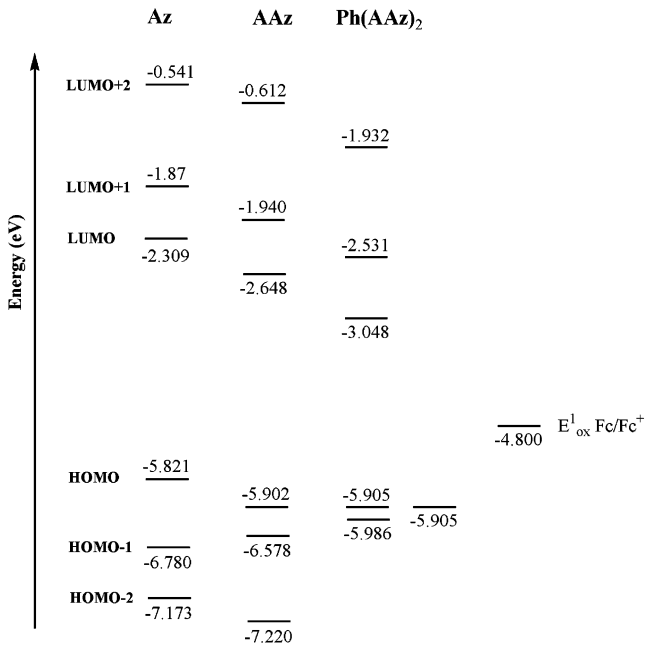

Figure 4. Evolution of the absolute DFT/B3LYP/6-31G** energies for the orbitals around the gap upon increasing branching of Az.

One cannot obviate the experimental finding that on going from Az to AAz the HOMO−LUMO band varies 34 nm, and only 36 nm to $Ph(AAz)_2$. First, a delocalization effect (cofacial π type interaction) is valid for the larger systems, but it is hard to assume for a 34 nm red shift after increasing the molecule size with a triple bond. Due to the withdrawing nature of the sp hybridization of the C≡C bond versus the sp^2 of the C=C bonds, one can expect a coaxial electrostaticlike interaction, which is well-known to cause important bathochromic displacements (intramolecular charge-transfer features) of the $\pi-\pi^*$

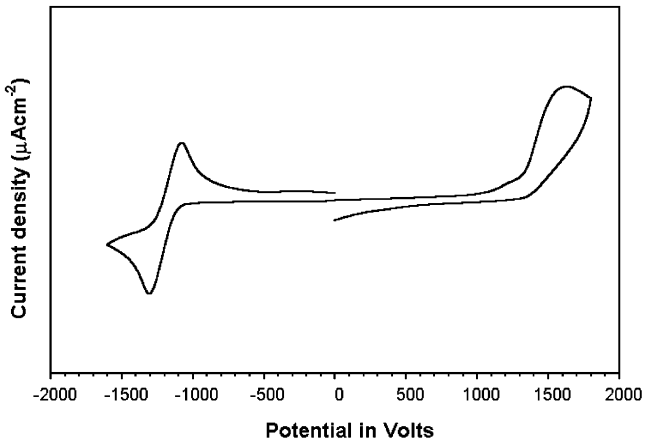

Figure 5. Cyclic voltammetry wave of $Ph(AAz)_2$ in *o*-dichlorobenzene containing tetrabutylammonium tetrafluoroborate (0.1 M).

band depending of the relative electronegativity (donor−acceptor character) of the interacting groups. For instance, this is the case for push−pull molecules built up with electron donor and electron acceptor groups connected trough a conjugated C═C/C−C path that changes their $\pi-\pi^*$ band up to 100 nm depending of the electrostatic nature of the donors and acceptors.[15] In fact, if this electrostatic effect is ignored when considering $Ph(Az)_2$, then the spectrum just changes 8 nm with respect to Az, which outlines the effect of the inclusion of triple bonds in the optical and electronic properties of these derivatives. Second, the minimal difference between AAz and $Ph(AAz)_2$ can have at least two reasons: (a) this visible band evolves from an almost exclusively HOMO−LUMO feature in Az and in AAz to a multielectronic promotion in $Ph(AAz)_2$, which likely blueshifts the final appearance of the longest wavelength one could expect from the exclusive consideration of the HOMO and LUMO terms; (b) although not predicted by theory, one cannot fully neglect slight distortions from the planarity for the larger molecules, especially in solution, which can influence the absorption spectrum of $Ph(AAz)_2$ but not that of AAz due to the cylindrical shape of the triple bond.

For the series of branched compounds around the central phenyl ring, the progressive narrowing of the energy gap already predicted by theory and due to the delocalization of the LUMO over larger molecular domains that leads to its energetic stabilization (the energy of the HOMO is almost indifferent to the branching) well accounts for the observed red shift of the longest wavelength band on going from $Ph(AAz)_2$ (538 nm) to $Ph(AAz)_3$ (542 nm), $Ph(AAz)_4$ (548 nm), and $Ph(AAz)_6$ (558 nm).

IV. Electrochemical Data

The electrochemical properties of these molecules can also be addressed by consideration of the shape and energy of their frontier molecular orbitals. It is extensively known that the azulene system itself has a tendency to stabilize cations, as well as anions, owing to its remarkable polarizability. Our molecules, however, are suitably functionalized with electron acceptor groups to better stabilize anions in detriment of their cationic counterpart.[3] However, it is relevant from a conceptual point of view to revise the characterization of their anodic processes as compared with the predictions of theory. As a representative case, Figure 5 shows the cyclic voltammetry (CV) of $Ph(AAz)_2$ in the full electrochemical range. The attachment of two ester electron-withdrawing groups positively shifts the oxidations processes from around +1 V in the nonsubstituted azulene derivatives to +1.60 V in $Ph(AAz)_2$, +1.75 V in $Ph(AAz)_3$ (we call the attention in this value), +1.55 V in $Ph(AAz)_4$, and +1.57 V in $Ph(AAz)_6$ versus Ag/Ag^+ using Fc/Fc^+, which discharges at +0.26 V, as an internal reference.[4,5] Because the energy of the Fc/Fc^+ can be estimated to be −4.80 eV with respect to the vacuum level, it is possible to qualitatively compare the electrochemical potentials with the energy of the frontier orbitals for the neutral molecule within Koopman's approach, which briefly states that oxidation proceeds through electron extraction from the HOMO whereas reduction consists of the accommodation of new electrons in the LUMO without any electronic or structural reorganization of the system. The electron pinning of the p_z carbon electrons in the Az moiety for their HOMOs, namely, scarce dependence on their wavefunction shape and energy for all of the compounds, explains quite well the little dependence of the first oxidation potentials on the branching of the central phenyl ring.

Cathodic processes present a rather different scenario. Due to reductions related to the LUMOs, which are due to its delocalized nature that strongly depends on energy of the branching of the system, the largest molecule, $Ph(AAz)_6$, is able to accommodate in only one step in the CV up to six electrons. The large extension of its LUMO efficiently permits it to mitigate the electronic repulsions between the injected negative charges. In this sense, there is a clear dependence on the number of injected electrons in the CV with the number of arms of the molecule; hence, $Ph(AAz)_2$ has a two-electron process at −1.19 V, and $Ph(AAz)_3$ shows a three-electron process at −1.39 V whereas the reduction of $Ph(AAz)_6$ consists of a six electron incorporation at −1.28 V. For $Ph(AAz)_4$, its CV presents two two-electron reductions at −1.08 and −1.28 V. The processes at −1.19 V in $Ph(AAz)_2$ and −1.08 V in $Ph(AAz)_4$ allow the comparison of the dependence of the reductions as a function of the branching of the molecules. Again, as the LUMO is more extended, the potential values decrease.

The reductions however are not only modulated by the number of azulene moieties, but one cannot obviate the role of the acetylene groups because their electron-withdrawing nature confers the molecule more acceptor character as more triple bonds are present. This is clearly shown by comparisons of the reduction potentials of the branched molecules with and without acetylenes: −1.19 V/−1.30 V in $Ph(AAz)_2/Ph(Az)_2$ and −1.08 V/−1.31 V in $Ph(AAz)_4/Ph(Az)_4$.

At this point of the discussion, it must be noted that among the whole set of compounds only the CV of $Ph(AAz)_3$ is irreversible in the cathodic branch. Furthermore, its oxidation potential, +1.75 V, does not correlate with those of its parents. As it will be shown in the next sections, the stabilization of the dianionic forms requires the formation of a cumulenic structure for the acetylene spacers through the inner phenyl ring. The formation of the cumulated double bond sequences is precluded for $Ph(AAz)_3$ because the conjugated path is not in a linear disposition.[17] In contrast to linear conjugated chromophores, cross-conjugated molecules generally display reduced π-electron conjugation and electron affinity.

V. Raman Spectra: Assignment and Interpretation

Despite the large number of atoms in these systems, their experimental Raman spectra in the solid state display only 10−12 well-resolved bands, which can be in principle surprising to the view of the nonspecialist. This unexpected appearance can be justified by taking into account that when Franck−Condon scattering in the Raman phenomenon is predominant (this is the case for most polyconjugated systems) only totally sym-

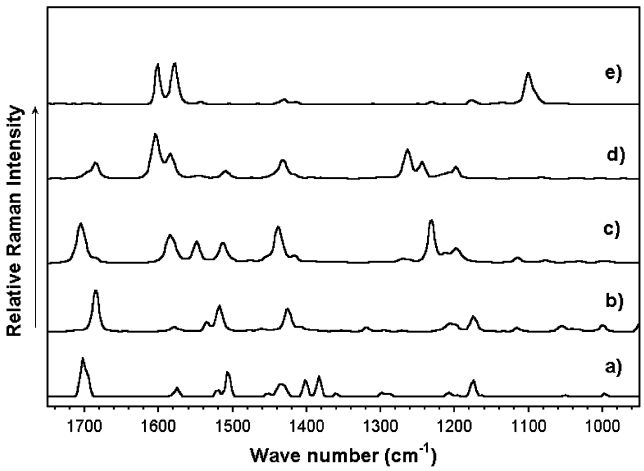

Figure 6. Theoretical DFT/B3LYP/6-31G** Raman spectrum of (a) Az and the experimental ones of (b) Az, (c) $(Az)_2$, (d) $Ph(Az)_2$, and (e) $Ph(AAz)_2$.

metric modes are found to be selectively enhanced, whereas the rest of the modes become weak or almost undetectable. Furthermore, among the totally symmetric modes, only those that somewhat resemble the evolution of the molecular structure from the ground electronic state to the first excited state are selectively enhanced (they carry out the largest variations of the molecular polarizability, which translates into large or very large Raman activity). This is clearly shown by the vibronic structure of their longest wavelength electronic absorption bands; hence, for $Ph(AAz)_4$ the maximum of the band is measured at 541 nm, and its first vibronic peak is recorded as a shoulder at 592 nm, therefore spaced by 1590−1600 cm^{-1} which closely corresponds to the wavenumber of one of the most intense bands of its Raman spectrum. This reasoning allows the direct comparison of the spectra in the series, despite their different molecular symmetry, whereas the simplicity of the spectra leads to a facile comparison of the features which predominantly arise from the conjugated path.

The B3LYP/6-31G** theoretical Raman spectrum of Az (having methyl instead of hexyl groups) has been obtained to help with the assignment of the experimental features and is shown in Figure 6 together with the FT-Raman spectra of Az, $(Az)_2$, $Ph(Az)_2$, and $Ph(AAz)_2$, thus leading us to follow the evolution of the main scatterings as a result of the different grafting of the azulene group.

The band at 1579 cm^{-1} in Az correlates with the theoretical feature at 1575 cm^{-1}, which, based on its eigenvector in Figure 7, can be described as a C—C stretching vibration of the seven-membered ring, excluding the two bonds involving the atom to which the acetylenes are attached. This vibration appears at 1580 cm^{-1} in AAz and 1578 cm^{-1} in $Ph(AAz)_2$. Figure 8 displays the evolution of the theoretical B3LYP/6-31G** bond distances on going from Az to $Ph(AAz)_2$ and to $Ph(AAz)_4$. In accordance with the Raman line change, it is observed that the bonds involved in this vibration scarcely modify its nature because their averaged bond lengths change is only 0.003 Å.

The weak peak at 1535 cm^{-1} in Az (calculated at 1519 cm^{-1}) evolves to 1548 cm^{-1} in $(Az)_2$, to 1544 cm^{-1} in $Ph(Az)_2$, and to 1543 cm^{-1} in $Ph(AAz)_2$ and is due to a coupled β(C—H) deformation and ν(C—C) stretching of the seven-membered ring. The substitution of the Az group can somewhat preclude the side movement of the C—H bond by which more energy is required to make the deformation, thus expecting a frequency upshift. Contrarily, a progressive downshift is observed for the frequency line at 1520−1500 cm^{-1} from 1518 cm^{-1} in Az to

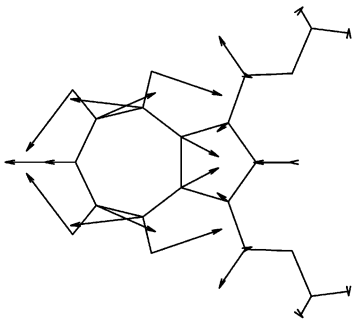

Theor.: 1575 cm^{-1}

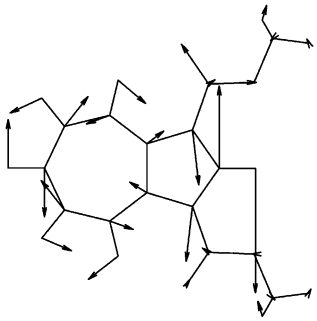

Theor.: 1506 cm^{-1}

Figure 7. DFT/B3LYP/6-31G** vibrational eigenvectors associated with some Raman lines of the theoretical spectrum of Az (methyls instead of hexyl groups).

1503 cm^{-1} in $Ph(AAz)_2$. This set of bands correlates with the theoretical feature at 1506 cm^{-1} that mainly corresponds to a C—C stretching of the two bonds of the carbon atom to which the triple bond is attached (Figure 7). As deduced from Figure 8, the greatest bond length changes take place just for these two bonds, which lengthen by around 0.017 Å, accounting for the large frequency decrease of its associated C—C stretching vibration. The π cofacial coupling through the p_z orbitals and the coaxial electron donor−acceptor interactions between the groups are likely responsible for the theoretically predicted relaxation of the structure.

The pair of bands at 1428 and 1408 cm^{-1} in Az, 1430 and 1413 cm^{-1} in AAz, 1432 and 1416 cm^{-1} in $Ph(Az)_2$, and 1431 and 1414 cm^{-1} in $Ph(AAz)_2$ are associated with the theoretical bands at 1428 and 1401 cm^{-1}, respectively, the first one corresponding to a vibration of the hexyl carboxylate groups. For these groups, the frequency and intensity of their bands are dependent on the orientation of the two C═O groups relative to the Az moiety. Between them and relative to the Az moiety, these C═O groups can be disposed in syn up, syn down, or anti configurations as illustrated in Figure S1. Quantum chemical calculations of the vibrational spectra of these conformers of Az have been carried out, yielding the result that the syn down conformer better suits the experimental spectra, although spectroscopic signatures of the others also can be found. This fact can reveal the conformational disorder associated with the hexyloxycarbonyl chains otherwise detected by the temperature-dependent X-ray diffraction data. This conformational analysis serves also to explain the behavior of the ν(C═O) Raman band around 1700−1680 cm^{-1}, which consists of the appearance of a single or double band depending on the relative syn/anti conformations (Figure S1). The weak band at 1408 cm^{-1} (theoretical at 1401 cm^{-1}) now corresponds with the δ(C—H)

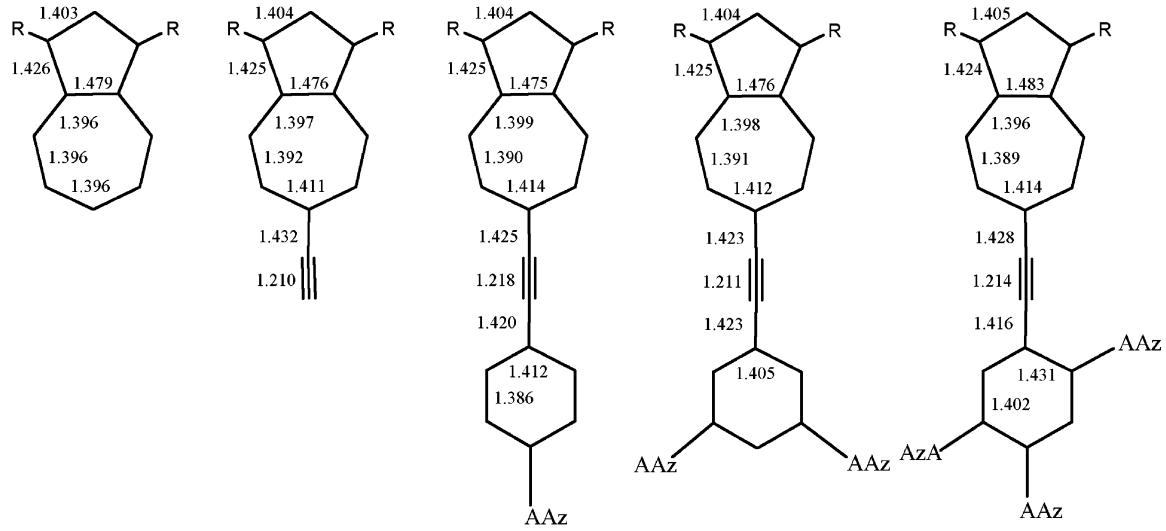

Figure 8. Evolution of the DFT/B3LYP/6-31G** geometries on passing from Az to $Ph(AAz)_2$ and to $Ph(AAz)_4$.

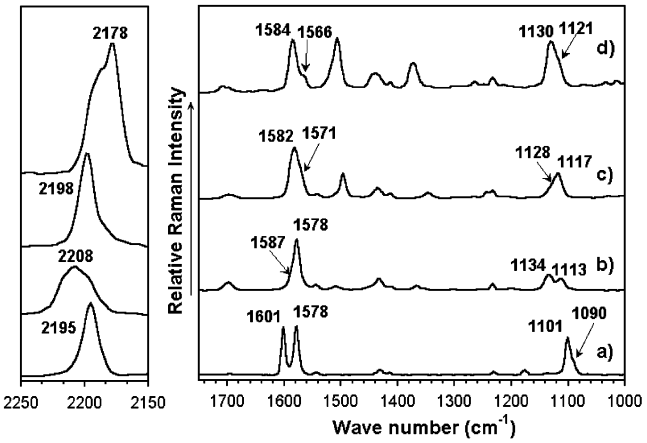

Figure 9. FT-Raman spectra in solid state of (a) $Ph(AAz)_2$, (b) $Ph(AAz)_3$, (c) $Ph(AAz)_4$, and (d) $Ph(AAz)_6$.

vibrations of the two rings coupled with the corresponding ν(C—C) stretchings.

The set of weak bands at 1280−1260 cm^{-1} emerges from almost pure antisymmetric ring δ(C—H) vibrations whereas those in the interval 1180−1160 cm^{-1} belong to the symmetric δ(C—H) counterpart. Between these two sets of bands, Raman lines due to ν(C—C) stretching of single bonds start to appear in the spectra of the azulene derivatives. Particularly important is the Raman band at 1100 cm^{-1} in $Ph(AAz)_2$, absent in the other spectra of Figure 6, which can be assigned to the stretching motion of the bond that connects the acetylene group and the azulene moiety. The low frequency for this band is a consequence of its single bond character (theoretical bond length of 1.425 Å in $Ph(AAz)_2$). This band is structured with a shoulder at its low energy side that can likely arise from the homologous ν(C—C) vibration of the bond connecting the triple bond with the central phenyl ring (see next discussion and Figures 10 and 11).

VI. Raman Spectra of the Branched Systems

Figure 9 displays the FT-Raman spectra of the four branched compounds with acetylene groups. The most intense bands of the spectra are measured as well-resolved Raman peaks at around 2190 cm^{-1} that can be described as fully in-phase C≡C stretching vibrations, ν_s(C≡C), measured at 2195 cm^{-1} in $Ph(AAz)_2$, 2208 cm^{-1} in $Ph(AAz)_3$, 2198 cm^{-1} in $Ph(AAz)_4$, and 2178 cm^{-1} in $Ph(AAz)_6$. This frequency evolution might be due to the combination of two main effects.

(a) For $Ph(AAz)_2$ and $Ph(AAz)_3$, calculations predict their molecular structure to be planar because the substitution pattern in the former is more favorable to π-electron delocalization through the phenyl core due to cross conjugation. As a result, there exists a greater relaxation of the structure in $Ph(AAz)_2$; hence, its triple bond length is the largest one, which supports the low frequency appearance of its ν_s(C≡C). Regarding $Ph(AAz)_4$, however, the azulene groups are slightly distorted by steric hindrance relative to the central ring by 23° according to its theoretical B3LYP/6-31G** optimized geometry. The structure of $Ph(AAz)_4$ can be viewed as that of two fused $Ph(AAz)_2$ in a cross-conjugated pattern, which, in fact, seems to prevent effective core π-electron deslocalization, giving rise to a charge localization as deduced by the shortening/lengthening of the triple/single bonds of the acetylene spacer. As a matter of fact, the ν_s(C≡C) frequency in $Ph(AAz)_4$ is slightly higher than that found in $Ph(AAz)_2$.

(b) Another perspective that one may reasonably argue is that, owing to the sp hybridization of the acetylide bonds, these could be viewed as weak electron-accepting or -withdrawing groups relative to their sp^2 counterparts (previously referred as the coaxial electron donor−acceptor interactions). This charge polarization effect can induce a confinement on the π-electron density in the acetylene moiety, which, likely due to the repulsion of the accumulated charge, can cause a partial loss of the triple bond character, thus inducing and shifting its ν_s(C≡C) Raman band to lower wavenumbers. This reasoning is also supported by the theoretical calculations through the consideration of the total negative charge in the C≡C bond (sum of the Mülliken atomic charges of the two sp carbon atoms), which amounts to be −0.067 e in $Ph(AAz)_2$ and −0.080 e in $Ph(AAz)_3$.

Now, we will analyze the modifications to the central benzene. To clarify the assignment of the bands, the theoretical spectrum of $Ph(AAz)_2$ also has been obtained and shown in Figure 10. The experimental band at 1601 cm^{-1} of $Ph(AAz)_2$, which relates with the theoretical feature also at 1601 cm^{-1}, is due, on the basis of its eigenvector (Figure 11), to a skeletal C—C stretching vibration of the phenyl ring that mainly involves the C—C bonds with double bond character (Figure 8). This band is recognized at 1601 cm^{-1} in $Ph(AAz)_2$, 1587 cm^{-1} (shoulder) in $Ph(AAz)_3$, 1571 cm^{-1} (shoulder) in $Ph(AAz)_4$, and 1566 cm^{-1} in $Ph(AAz)_6$. The lowest wavenumber corresponds

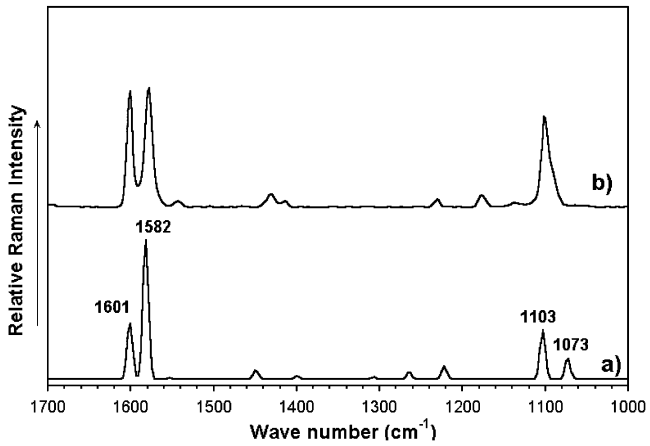

Figure 10. Comparison between the theoretical DFT/B3LYP/6-31G** Raman spectrum of $Ph(AAz)_2$ (a) and its experimental one (b).

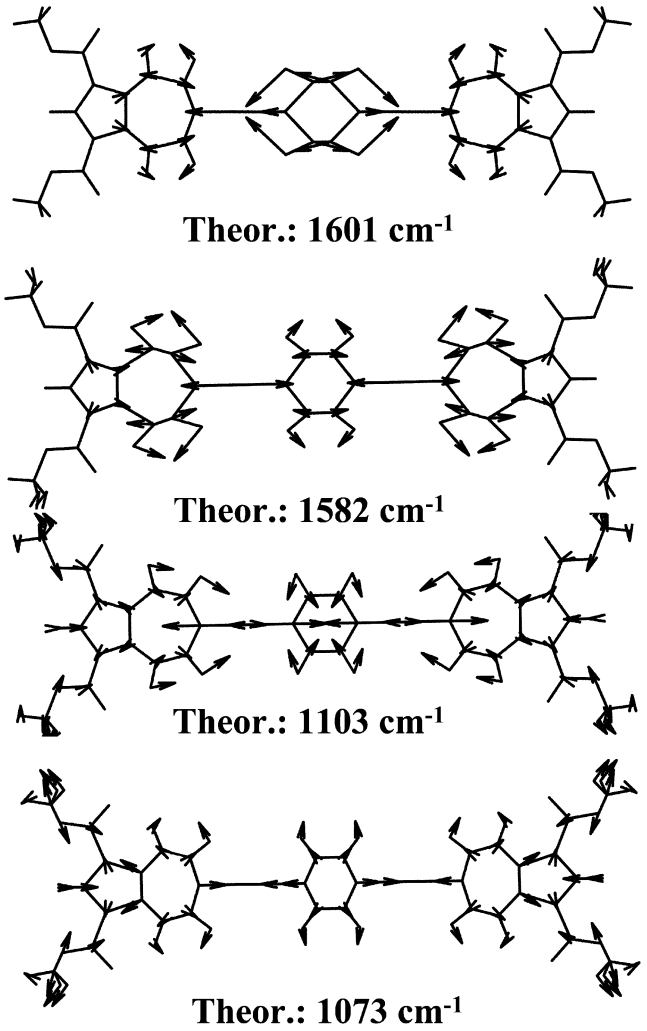

Figure 11. DFT/B3LYP/6-31G** vibrational eigenvectors associated with some Raman lines of the theoretical spectrum of Az (methyls instead of hexyl groups).

precisely to the most branched compound, which reveals that this is the most electron-deficient phenyl ring in the series. The theoretical B3LYP/6-31G** Mülliken atomic charges provide evidence for the increment of positive charge or removal of electron charge density on the central phenyl ring with the increasing number of peripherical electron-withdrawing triple bonds: +0.106 e in $Ph(AAz)_2$, +0.148 e in $Ph(AAz)_3$, or +0.162 e in $Ph(AAz)_4$. This explanation is supported by the data for the branched molecules without triple bonds where the ν(C═C) vibrations of the phenyl ring appear at higher wavenumber values than those found for their acetylene bridged parents: 1604 cm^{-1} in $Ph(Az)_2$, 1597 cm^{-1} (shoulder) in $Ph(Az)_3$, and 1595 cm^{-1} in $Ph(Az)_4$.

We have very recently studied a homologous molecule of $Ph(AAz)_6$ but with phenyl terthienyl groups instead of the azulenes for which the ν(C═C) phenyl band appears 8 cm^{-1} upshifted at 1574 cm^{-1}.[16] For this thienyl derivative, a weak coupling has been observed between the core (phenyl and acetylene moieties) and the outermost groups. This seems to support the existence of a effective electronic interaction among the various building blocks of our derivatives.

The intense band at 1578 cm^{-1} in $Ph(AAz)_2$, 1578 cm^{-1} in $Ph(AAz)_3$, 1582 cm^{-1} in $Ph(AAz)_4$, and 1584 cm^{-1} in $Ph(AAz)_6$ (theoretically predicted at 1582 cm^{-1} in the spectrum of $Ph(AAz)_2$) and the bands at 1503 cm^{-1} in $Ph(AAz)_2$ and $Ph(AAz)_3$ and 1506 cm^{-1} in $Ph(AAz)_6$ (which evolve from the 1518 cm^{-1} band in Az) are due to C—C stretching vibrations involving the seven-membered ring. The bands at higher values involve the stretching of the bonds with lengths in the range 1.389−1.399 Å and are less affected by the presence of the triple bond. However, the lower frequency bands correspond with bond stretchings with more single bond character (1.396−1.414 Å). As can be observed in Figure 8, there exists a relationship between the bond lengths and the Raman frequencies observed in the experimental spectra as a function of the branching.

The carbon atom of the Az group, which is directly connected to the triple bond in AAz, bears a total Mülliken atomic charge of +0.057 e, which evolves from +0.024 e in Az and goes to +0.072 e in $Ph(AAz)_2$. This charge polarization effect is, however, stronger because the charge withdrawal does affect the whole seven-membered ring, which changes its total charge from +0.244 e in Az to +0.253 e in $Ph(AAz)_2$ or +0.263 e in $Ph(AAz)_3$. Regarding bond lengths for this ring, it seems to exhibit a lack of aromaticity upon branching of the central benzene as expected by the increasing of the differences of the consecutive C—C bond lengths of the seven-membered ring.

Another interesting feature is the bands around 1100 cm^{-1}, which appear as a doublet for the molecules: 1101 and 1090 cm^{-1} in $Ph(AAz)_2$, 1134 and 1113 cm^{-1} in $Ph(AAz)_3$, 1128 cm^{-1} (shoulder) and 1117 cm^{-1} in $Ph(AAz)_4$, and 1130 and 1121 cm^{-1} (shoulder) in $Ph(AAz)_6$. The experimental doublet for $Ph(AAz)_2$ relates well with the bands at 1103 and 1073 cm^{-1} in its theoretical spectrum which are due to ν(C—C) stretching vibrations of the whole acetylene spacer with different contributions to the C—C bond connecting to the azulene or to the central benzene, respectively (Figure 11). For this doublet, the wavenumber separation is progressively decreasing as the molecule grows, which can be a proof of the increase in cyanine character by the spacer, which consists of the equalization of its bonds. This is except for $Ph(AAz)_3$ in which the cyanine−cumulenic structure is hindered by cross conjugation.

The analysis of the modulation of the electronic structure of these molecules is completed by addressing the case of its dependence on the redox state. As seen before, these systems are mainly conceived as electron acceptors, which this section is devoted to matching spectroscopic and theoretical data on the stable reduced forms. UV−vis spectroelectrochemical experiments have been carried for $Ph(AAz)_4$ using *o*-dichlorobenzene containing Bu_4NBF_4 (0.1 M) at room temperature under electrochemical reduction conditions. Only one well-resolved isobestic point was observed, indicating the formation

of a new species in solution. Its 300−900 nm electronic spectrum shows a peak around 520 nm with a large absorbance tail toward the near-IR region. TDDFT calculations of the dianion and tetraanion species of $Ph(AAz)_4$ were carried out and found that the best fitting with experiments is found for $[Ph(AAz)_4]^{2-}$. The calculation predicts the most intense band to appear at 505 nm with a oscillator strength of 2.6 although there exists another theoretical feature at 1024 nm ($f = 1.46$) that has no experimental counterpart in the region studied up to 1200 nm. Regarding the neutral system, optimized geometry for this dianion consists of a planarization of the azulene moieties in respect to the central phenyl ring. However, the analysis of the Mülliken atomic charges reveals that this innermost ring, which is predicted to be electron deficient for the neutral case, is the main drain of negative charge in the reduced form because it goes from +0.129 e in the noncharged molecule to −0.060 e in $[Ph(AAz)_4]^{2-}$. Although the azulene groups are conceived as the driving force for the reduction processes, the effective interaction between the building blocks of the molecule, particularly for the LUMOs, makes the injected charge of the dianions shared by the whole molecule. In this sense, theoretical bond lengths show the largest changes to affect the acetylene moieties, which tend to acquire a cumuleniclike structure because they are lengthened and their connecting single bonds are considerably shortened.

VII. Thermospectroscopic Study

The thermal features of these materials are of key interest given their liquid crystalline properties. Phase transition behavior for these molecules have been already examined in the range between room temperature and decomposition. Apart from the particular existence of polymorphs, it is worth mentioning that the molecules organize in columnar mesophases independently of the particular structure of each phase. In fact, it has been found by NMR measurements that these molecules easily aggregate in solution, which has been confirmed here by means of electronic absorption measurements at different temperatures in solution. The UV−vis spectra at temperatures below 0 °C become much broader and red shifted toward the near-IR region. A similar behavior has been found for a series of related molecules consisting of a flat aromatic core and peripheral hydrocarbon side chains, namely, octakis(alkoxy)-substituted phthalocyanines, which also self-organize into columnar stacks.[6a] In this case, the broadening of the electronic band accompanied by the red shift is explained as a consequence of the full planarization of the molecule in the stack from a sandwiched concave structure after phase transition on cooling. The HOMO → LUMO transition character of the electronic feature in our derivatives makes this band sensitive to the planarization of the external azulenes with respect to the central core, which could address our observations in the UV−vis spectra at low temperatures. Apart from the description at a molecular scale, one cannot obviate supramolecular effects such as the aggregation of the molecules in solution as observed by ^{1}H NMR. The broadening of the absorption band due to intermolecular contacts by aggregation, which is favored at low temperatures, is another factor explaining our experimental results.

Figure 12 shows the Raman spectra of $Ph(AAz)_6$ in solid state as a function of the temperature. The ν(C≡C) line, consisting of one broad Raman band at room temperature, splits into a few components for the spectra obtained at −90 and −170 °C. The Raman band of the seven-membered ring around 1587 cm^{-1} at room temperature shifts from 1588 cm^{-1} at −170 °C to 1579 cm^{-1} at 150 °C. Greater changes in the Raman lines are measured for the vibrations mainly involved in the conjugational path, namely, the band around 1505 cm^{-1} that goes from 1508 cm^{-1} at −170 °C to 1502 cm^{-1} at 150 °C and the band around 1100 cm^{-1} that changes by 7 cm^{-1}. The rest of the bands scarcely vary their peak positions by 2−3 cm^{-1}. For this system, columnar mesomorphism was observed at 77.3 °C; therefore the changes in the spectra above room temperature can be attributed to the phase transition from the crystals to the columnar mesophase (Col_{ho}), which is characterized by a high viscosity. The changes in the spectra below 0 °C can be due to (a) Davidov splitting of the crystalline phase due to strong interaction of the neighbor molecules in the unit cell, which is well-known to appear especially at low or very low temperatures and (b) a certain degree of planarization of the molecules, even in solid state upon cooling, which otherwise could favor the Davidov effect.

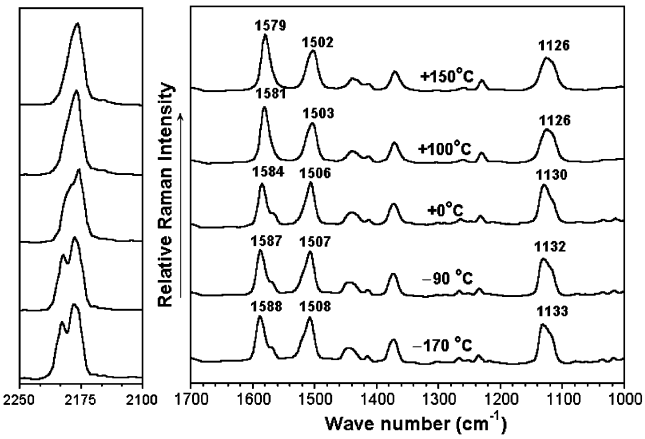

Figure 12. Thermal evolution of the Raman spectrum of $Ph(AAz)_6$ in the solid state.

If the interaction between stacked molecules in the columnar mesophase or in the unit cell occurs by cofacial contact of the electronic clouds, then one can expect the frontier orbitals to be mostly influenced and the conjugated path due to their π nature. Therefore, it is reasonable to find the largest changes in the Raman frequencies for normal modes involving atoms connected through double or triple bonds in the conjugated spine.

VIII. Conclusions

A series of branched poly(6-azulenylethenyl)benzene derivatives consisting of a central benzene ring surrounded by acetylene-bridged 1,3-bis(*n*-hexyloxycarbonyl) azulene arms has been investigated by combining UV−vis and Raman spectroscopies, electrochemistry, in situ spectroelectrochemistry, and theoretical calculations. The relevance of these compounds is that they exemplify a new principle for multielectron redox behavior while at the same time that they display liquid crystalline properties. Their optical and electrochemical features have been explained with the help of calculations with respect to the π nature and extension of the LUMOs, the key factors that modulate these properties. The principal role of the acetylene groups has been interpreted as contributing an electron-withdrawing effect over its chemical environment, which certainly modulates the optical and electrochemical features of the molecules. In the sense that the HOMO is located at the periphery of the molecules and that the LUMO also extends in the central part, these molecules can be regarded as antennae systems in which an effective transporting of charge and optical signals from the outermost sites to the central core might occur.

The analysis of the Raman spectra allows us to study and understand detailed aspects of the structure of these interesting molecules on the basis of the behavior of the vibrational bands as microscopic probes of the structure. With an increase in the branching pattern, the electronic structure of the molecules seems to be mostly affected at the level of the central phenyl core plus the acetylene bridges, whereas the outermost groups are less affected probably because these electronic changes are mitigated within the big azulene moiety. Reduced species are characterized by the appearance of double bond cumulated structures within the acetylenic spacers, which gives rise to a planarization of the molecules with respect to the neutral molecules upon negative charging. Extensive electronic interaction between the molecules in solution and molecules in the solid state related with the their mesomorphism and liquid crystalline behavior has been observed.

Acknowledgment. J.C. is grateful to the Ministerio de Ciencia y Tecnología (MCyT) of Spain for a Ramón y Cajal research position of Chemistry at the University of Málaga. The present work was supported in part by the Dirección General de Enseñanza Superior (DGES, MEC, Spain) through the research project BQU2003-03194. We are also indebted to Junta de Andalucía (Spain) for funding for our research group (FQM-0159). R.P.O. thanks the MEC for a personal grant.

Supporting Information Available: Experimental and theoretical Raman spectra for three conformers of Az. This material is available free of charge via the Internet at http://pubs.acs.org.

References and Notes

(1) (a) Monk, P. M. S., Mortimer, R. J. Rosseinsky, D. R. *Electrchromism: Fundamentals and Applications*; VCH: Weinheim, Germany, 1995. (b) Chandrasekhar, S. *Liq. Cryst.* **1993,** *14*, 3. (c) Demus, D. In *Handbook of Liquid Crystals*; Demus, D., Goodby, J., Gray, G. W., Spiess, H.-W., Vill, V., Eds.; Wiley-VCH: Weinheim, 1998; Vol. 1, Chapter VI. (d) Colling, P. J. Hird, M. In *Introduction to Liquid Crystals: Chemistry and Physics*; Taylor & Francis Ltd.: London, 1977; Chapter IV.

(2) Deuchert, K.; Hünig, S. *Angew. Chem., Int. Ed. Engl.* **1978**, *17*, 875.

(3) Ito, S.; Inabe, H.; Morita, N.; Ohta, K.; Kitamura, T.; Imafuku, K. *J. Am. Chem. Soc.* **2003**, *125*, 1669.

(4) Ito, S.; Inabe, H.; Okujima, T.; Morita, N.; Watanabe, M.; Harada, N.; Imafuku, K. *Tetrahedron Lett.* **2001**, *42*, 1085.

(5) (a) Ito, S.; Okujima, T.; Morita, N. *J. Chem. Soc., Perkin Trans.* **2002**, *1*, 1986. (b) Ito, S.; Kubo, T.; Morita, N.; Ikoma, T.; Tero-Kubota, S.; Tajiri, A. *J. Org. Chem.* **2003,** *68*, 9753.

(6) (a) Van de Craats, A. M.; Warman, J. M.; Hasebe, H.; Naito, R.; Ohta, K. *J. Phys. Chem. B* **1997**, *101*, 9224. (b) Van de Craats, A. M.; Warman, J. M.; Müllen, K.; Geerts, Y.; Brand, J. D. *Adv. Mater.* **1998**, *10*, 36.

(7) Zerbi, G.; Castiglioni, C.; Del Zoppo, M. *Electronic Materials: The Oligomer Approach*; Wiley-VCH: Weinheim, 1998; p 345.

(8) Rumi, M.; Zerbi, G.; Müllen, K.; Müller, G.; Rehahn, M. *J. Chem. Phys.* **1997**, *106*, 24.

(9) Kozlowski, P. W.; Rauhut, G.; Pulay, P. *J. Chem. Phys.* **1995**, *103*, 5654.

(10) Martin, J. M. L.; El-Yazal, J.; François, J. P. *J. Phys. Chem.* **1996**, *100*, 15358.

(11) Bandyopadhyay, I. *J. Mol. Struct.* **2002**, *618*, 59.

(12) (a) Rauhut, G.; Pulay, P. *J. Phys. Chem.* **1995**, *99*, 3093. (b) Pulay, P.; Fogarasi, G. *J. Am. Chem. Soc.* 1983, *105*, 7037. (c) Scott, A. P.; Radom, L. *J. Phys. Chem.* **1996**, *100*, 16502.

(13) Frisch, M. J.; Trucks, G. W.; Schlegel, H. B.; Scuseria, G. E.; Robb, M. A.; Cheeseman, J. R.; Zakrzewski, V. G.; Montgomery, J. A.; Stratman, R. E.; Burant, S.; Dapprich, J. M.; Millam, J. M.; Daniels, A. D.; Kudin, K. N.; Strain, M. C.; Farkas, O.; Tomasi, J.; Barone, V.; Cossi, M.; Cammi, R.; Mennucci, B.; Pomelli, C.; Adamo, C.; Clifford, S.; Ochterski, G.; Petersson, A.; Ayala, P. Y.; Cui, Q.; Morokuma, K.; Malick, D. K.; Rabuck, A. D.; Raghavachari, K.; Foresman, J. B.; Cioslowski, J.; Ortiz, J. V.; Stefanov, B. B.; Liu, G.; Liashenko, A.; Piskorz, I.; Komaromi, I.; Gomperts, R.; Martin, R. L.; Fox, D. J.; Keith, T.; Al-Laham, M. A.; Peng, C. Y.; Manayakkara, A.; Gonzalez, C.; Challacombe, M.; Gill, P. M. W.; Johnson, B. G.; Chen, W.; Wong, M. W.; Andres, J. L.; Head-Gordon, M.; Replogle, E. S.; Pople, J. A. *Gaussian 98*, Revision A.7; Gaussian, Inc.: Pittsburgh, PA, 1998.

(14) (a) Gross, E. K. U.; Kohn, W. *Adv. Quantum Chem.* **1990**, *21***,** 255. (b) Gross, E. K. U.; Ullrich, C. A.; Gossmann, U. J. In *Density Functional Theory*; Gross, E. K. U., Driezler, R. M., Eds.; Plenum Press: New York, 1995; p 149. (c) Francl, M. M.; Pietro, W. J.; Hehre, W. J.; Binkley, J. S.; Gordon, M. S.; Defrees, D. J.; Pople, J. A. *J. Chem. Phys.* **1982**, *77*, 3654.

(15) Effenberger, F.; Würthner, F.; Steybe, F. *J. Org. Chem.* **1995**, *60*, 2082.

(16) Casado, J.; Pappenfus, T. M.; Mann, K. R.; Hernández, V.; López Navarrete, J. T. *J. Chem. Phys.* **2004**, *120*, 11874.

(17) (a) Eisler, S.; Tykwinski, R. R. *Angew. Chem., Int. Ed.* **1999**, *38*, 1940. (b) Zhao, Y.; Ciuley, S. C.; Tykwinski, R. R. *Tetrahedron Lett.* **2001**, *42* (44), 7721.